

1309
34

3, N 21/5: 6/2313

NACA TN 2313

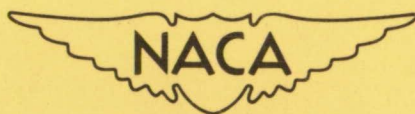
NATIONAL ADVISORY COMMITTEE FOR AERONAUTICS

TECHNICAL NOTE 2313

THE EFFECTS OF MASS DISTRIBUTION ON THE LOW-SPEED
DYNAMIC LATERAL STABILITY AND CONTROL
CHARACTERISTICS OF A MODEL WITH
A 45° SWEPTBACK WING

By Donald E. Hewes

Langley Aeronautical Laboratory
Langley Field, Va.



Washington

March 1951

CONF. STATE LIBRARY

MAR 19 1951

BUSINESS, SCIENCE
& TECHNOLOGY DEPT.

NATIONAL ADVISORY COMMITTEE FOR AERONAUTICS

TECHNICAL NOTE 2313

THE EFFECTS OF MASS DISTRIBUTION ON THE LOW-SPEED

DYNAMIC LATERAL STABILITY AND CONTROL

CHARACTERISTICS OF A MODEL WITH

A 45° SWEPTBACK WING

By Donald E. Hewes

SUMMARY

An investigation was carried out in the Langley free-flight tunnel to determine the trends in low-speed dynamic lateral stability and control characteristics produced by large variations in the mass distribution of a free-flying model with a 45° sweptback wing of taper ratio 0.6 and aspect ratio 4. The value of the relative-density factor was held constant in the investigation. Calculations of the characteristics of the lateral motions for the model were made to correlate the trends predicted by theory with those obtained from the flight tests.

In the investigation, increasing the rolling moment of inertia alone or increasing the rolling and yawing moments of inertia simultaneously was found to reduce both the controllability and oscillatory stability of the model. Increasing the yawing moment of inertia alone did not materially affect the stability of the model but made it more difficult to control. The general flight behavior became progressively worse as the moments of inertia were increased. Fairly good agreement was obtained between the trends predicted by theory and those obtained from the flight tests.

INTRODUCTION

Some investigations have shown that the stability and control characteristics of airplanes may be greatly affected by changes in mass distribution. One investigation of this type made to determine the effects of mass distribution on lateral stability and control of a model with an unswept wing is reported in reference 1. Recent trends in airplane design, however, have resulted in a range of mass-distribution parameters more extensive than that covered in reference 1. In addition, changes in the general configuration of airplanes, such as the use of

highly swept wings and long fuselages, have resulted in combinations of the aerodynamic parameters different from those of the model with the unswept wing used in that investigation. An investigation has therefore been carried out in the Langley free-flight tunnel on a free-flying dynamic model airplane with a sweptback wing to determine the trends in low-speed lateral stability and control produced by large variations in the mass distribution.

The model used in this investigation had a 45° sweptback wing of aspect ratio 4 and taper ratio 0.6 and a vertical tail having an area of 5 percent of the wing area. This configuration was chosen in order to obtain a combination of aerodynamic parameters typical of present-day airplane configurations. The investigation consisted of a series of flights with the yawing and rolling moments of inertia systematically increased. The weight was held constant throughout the investigation.

Calculations of the lateral stability and disturbed motions of the model were made to correlate the trends predicted by theory with those obtained from observation of the flight tests.

SYMBOLS

All stability parameters except as noted are based on the stability axes. The positive directions of the forces, moments, and angles are shown in figure 1 and the relation of the stability axes to the other reference axes is shown in figure 2.

S	wing area, square feet
\bar{c}	mean aerodynamic chord, feet
V	airspeed, feet per second
b	span, feet
l	longitudinal distance from center of gravity to center of pressure of vertical tail, measured parallel to longitudinal stability axis, feet
z	vertical distance from center of gravity to center of pressure of vertical tail, measured perpendicular to longitudinal stability axis, feet
q	dynamic pressure, pounds per square foot $\left(\frac{\rho}{2} v^2\right)$
ρ	air density, slugs per cubic foot

W	weight, pounds
g	acceleration due to gravity, feet per second per second
m	mass, slugs (W/g)
μ_b	relative-density factor ($m/\rho S b$)
α	angle of attack, degrees
η	angle of attack of principal axis of airplane, positive when longitudinal principal axis is above flight path at nose (fig. 2), degrees
ϵ	angle between body axis and principal axis, positive when body axis is above principal axis at nose (fig. 2), degrees
θ	angle between body axis and horizontal axis, positive when body axis is above horizontal axis at nose (fig. 2), degrees
γ	angle between flight path and horizontal axis, positive in climb (fig. 2), degrees
δ_a	aileron travel, degrees
δ_r	rudder travel, degrees
ψ	angle of yaw, degrees or radians
β	angle of sideslip, degrees or radians
ϕ	angle of bank, degrees or radians
k_{X_0}	radius of gyration about longitudinal principal axis, feet
k_{Z_0}	radius of gyration about vertical principal axis, feet
K_{X_0}	nondimensional radius of gyration about longitudinal principal axis (k_{X_0}/b)
K_{Z_0}	nondimensional radius of gyration about vertical principal axis (k_{Z_0}/b)

K_{XZ} nondimensional product-of-inertia parameter $\left((K_{Z_0}^2 - K_{X_0}^2) \cos \eta \sin \eta \right)$

N yawing moment, foot-pounds

L rolling moment, foot-pounds

Y lateral force, foot-pounds

C_L lift coefficient (Lift/qS)

C_n yawing-moment coefficient (N/qSb)

C_l rolling-moment coefficient (L/qSb)

C_Y lateral-force coefficient (Y/qS)

$$C_{n\beta} = \frac{\partial C_n}{\partial \beta} \text{ per radian}$$

$$C_{l\beta} = \frac{\partial C_l}{\partial \beta} \text{ per radian}$$

$$C_{Y\beta} = \frac{\partial C_Y}{\partial \beta} \text{ per radian}$$

$$C_{np} = \frac{\partial C_n}{\partial \frac{pb}{2V}} \text{ per radian}$$

$$C_{lp} = \frac{\partial C_l}{\partial \frac{pb}{2V}} \text{ per radian}$$

$$C_{Yp} = \frac{\partial C_Y}{\partial \frac{pb}{2V}} \text{ per radian}$$

$$C_{nr} = \frac{\partial C_n}{\partial \frac{rb}{2V}} \text{ per radian}$$

$$C_{l_r} = \frac{\partial C_l}{\partial \frac{rb}{2V}} \text{ per radian}$$

$$C_{Y_r} = \frac{\partial C_Y}{\partial \frac{rb}{2V}} \text{ per radian}$$

p	rolling angular velocity, radians per second
r	yawing angular velocity, radians per second
t	time, seconds
P	period of oscillation, seconds
$T_{1/2}$	time for amplitude of oscillation or spiral mode to decrease to one-half amplitude, seconds

APPARATUS

The investigation was carried out in the Langley free-flight tunnel, which is equipped for testing free-flying dynamic models. A complete description of the tunnel and its operation is given in reference 2. The static longitudinal and lateral aerodynamic parameters of the model were obtained from force tests run on the six-component balance described in reference 3. The dynamic lateral parameters of the model were obtained from force tests run on the six-component rotary balance described in reference 4.

A three-view drawing of the model used in the investigation is shown in figure 3 and the physical characteristics of the model are given in table I. The wing with 45° sweepback of the leading edge, taper ratio of 0.6, and aspect ratio of 4 was incorporated in the design because this plan form has been used in a coordinated investigation on the part of several research facilities and is considered typical of current design trends. The center of gravity of the model was located at 22 percent of the mean aerodynamic chord for all tests. A vertical tail having an area of 5 percent of the wing area was used throughout the investigation since this tail was found in preliminary tests to provide satisfactory directional stability for the basic condition of minimum inertias. The boom or stick type of fuselage was equipped with extensions at the nose and tail and also with a vertical mast extending above and below the center line at the center of gravity of the model. The fuselage extensions and mast were used to support the weights which were shifted to

vary the moments of inertia. The rudder and aileron control surfaces were interconnected to give a coordinated control movement and were operated by the pilot through a remotely controlled servomechanism in the model.

The model was ballasted with lead weights to obtain a wing loading of 4.32 pounds per square foot. The yawing and rolling moments of inertia were systematically increased by disposing these weights at various locations along the fuselage boom and the vertical mast. The pitching moment of inertia was likewise increased by this procedure. Because of the symmetry of the airplane, the effects of pitching moment of inertia on lateral stability are negligible and the changes in pitching moment of inertia were therefore disregarded in the investigation. The principal axes were aligned with the body axes ($\epsilon = 0^\circ$); therefore, shifting of the ballast along the body axes did not change the inclination of the principal axes of inertia. The weight of the model was kept constant so that the moments of inertia and the radii of gyration were solely a function of the displacement of the ballast weights from the center of gravity.

METHODS

Stability and Control Calculations

Calculations of the period and damping of the lateral oscillation were made by means of the equations presented in reference 5 for a series of moment-of-inertia conditions which covered the complete range of the flight test conditions. For all calculations, the aerodynamic parameters were held constant at the values shown in table II. Values for the lateral-stability parameters C_{Y_β} , C_{l_β} , and C_{n_β} were available from static force tests of the model with and without the vertical tail. Values for the parameters C_{Y_p} , C_{l_p} , and C_{n_p} of the wing-fuselage combination were available from rotary force tests and values for the parameters C_{l_r} and C_{n_r} of the wing were obtained by calculations based on equations presented in reference 6. Values for the vertical-tail contribution to the dynamic-stability parameters C_{l_r} and C_{n_r} were calculated from the equations given in table II. The value of the tail contribution to C_{n_p} was estimated by the method described in reference 7. The values of the tail contribution to C_{l_p} , C_{Y_r} , and C_{Y_p} were assumed to be zero.

The rolling and yawing motions of the model produced by a continuously applied rolling moment ($C_l = 0.001$) or a continuously applied yawing moment ($C_n = 0.001$) were calculated for four combinations of K_{X_0} and K_{Z_0} by means of the equations of motion presented in references 8 and 9. These motions were used to show the effects of K_{X_0} and K_{Z_0} on the response to aileron and rudder control.

Flight Testing Procedure

The damping of the lateral oscillation was observed for each test and a qualitative rating was assigned to each condition according to the relative degree of damping. Response of the model to lateral controls was observed and qualitative lateral-control ratings were assigned. A general-flight-behavior rating based on the relative lateral steadiness in flight and the amount of attention required by the pilot to fly the model in the center of the tunnel was also assigned to each test condition. These ratings are listed and defined in the following table:

Rating	Oscillatory damping	Rating	Lateral control	Rating	General flight behavior	
A	Stable, heavily damped	A	Good	A	Good	
B	Stable, moderately damped	B	Fair	B	Fair	
C	Stable, lightly damped	C	Poor	C	Poor	
D	Neutrally stable	D	Uncontrollable	D	Unflyable	
			} Satisfactory		} Satisfactory	
			} Unsatisfactory		} Unsatisfactory	

No attempt was made to assign ratings for spiral stability because it is difficult to evaluate in the free-flight tunnel and has been shown not to vary with mass distribution (references 1 and 10).

RANGE OF VARIABLES

All flight tests and calculations were made at a lift coefficient of 0.7 and with a wing loading of 4.32 pounds per square foot which corresponded to a value for the relative-density parameter μ_b of 20

at sea level. The aileron travel of the model was restricted to a total of 40° for the flight tests and the rudder travel was varied for each test to obtain the most satisfactory coordination of controls.

Since the total weight was held constant in the investigation, the results can be discussed in terms of the nondimensional radii of gyration in roll and yaw K_{X_0} and K_{Z_0} . The combinations of K_{X_0} and K_{Z_0} for which flight tests were made are given in table III and figure 4. The effects of changing K_{Z_0} without changes in K_{X_0} can be shown by comparison of conditions 1 through 3 and the effects of changing K_{X_0} without changes in K_{Z_0} can be shown by comparison of conditions 4 through 7.

Comparison of conditions 4 and 8 through 10 shows the effects of changing K_{X_0} and K_{Z_0} simultaneously. A change in K_{Z_0} with K_{X_0} and the total weight held constant corresponds to shifting equipment such as guns, ammunition, and fuel tanks forward and rearward of the center of gravity along the fuselage; whereas, changing both K_{X_0} and K_{Z_0} represents the shifting of equipment along the wing. Changing K_{X_0} with K_{Z_0} and the total weight held constant corresponds to relocation of equipment from along the fuselage to along the wing or to shifting weights vertically above and below the center of gravity.

Calculations for the period and the time to damp to one-half amplitude of the lateral oscillation were made for a range of values for K_{X_0} from 0.107 to 0.225 and for K_{Z_0} from 0.216 to 0.600. This range includes all the flight-test combinations and is represented in figure 4 as the region enclosed by the dashed line. The calculated motions of the model were made for the four combinations of K_{X_0} and K_{Z_0} which are represented by the diamond-shaped symbols in this same figure. These combinations are designated by the numerals I, II, III, and IV and are arranged so that a change from I to II or III to IV represents an increase in K_{X_0} , a change from I to III or II to IV represents an increase in K_{Z_0} , and a change from I to IV represents an increase in both K_{X_0} and K_{Z_0} .

In order to illustrate the practical range of these two variables, the combinations of K_{X_0} and K_{Z_0} for several current military airplanes are shown in figure 4 and are represented by the circular symbols. The range of K_{Z_0} covered in this investigation was extended beyond that defined by these circular symbols because of the expected trend in future

airplanes. The hatched diagonal line represents a boundary below which no combination of K_{X_0} and K_{Z_0} is expected to exist for any practical airplane, that is, where K_{X_0} is greater than K_{Z_0} .

RESULTS AND DISCUSSION

Results of recent investigations have shown that the effect on dynamic stability and control of any one particular parameter is usually dependent on other variables entering into the stability equation. The effects of mass distribution on lateral stability and control which were determined in this investigation therefore apply only to configurations and conditions generally similar to those used in the flight tests.

Oscillatory Stability

The qualitative damping ratings obtained from the flight tests are given in table III. The lateral oscillation was found to be stable for condition 1 and as K_{Z_0} was increased (by changing from condition 1 to condition 2 or 3) the damping of the oscillation increased slightly. The oscillation was stable for condition 4 and became less stable as K_{X_0} was increased (by changing from condition 4 to condition 5, 6, or 7) but did not become unstable even at the largest value of K_{X_0} . The effects of various simultaneous increases in K_{X_0} and K_{Z_0} (by changing from condition 4 to condition 8, 9, or 10) were found to be similar to those when K_{X_0} was increased independently; that is, the damping decreased as both K_{X_0} and K_{Z_0} were increased.

Results of the calculations of the period and time to damp for the lateral oscillation are presented in figure 5 in which P and $T_{1/2}$ are plotted against K_{X_0} for a series of K_{Z_0} values. This figure shows that the period increases as either K_{X_0} or K_{Z_0} or both increase but that the time to damp to one-half amplitude increases with increasing K_{X_0} and decreases with increasing K_{Z_0} . The time to damp can increase, decrease, or remain constant with simultaneous increases in K_{X_0} and K_{Z_0} depending on the ratio by which they are increased.

In reference 11 the effect of increasing K_{Z_0} on oscillatory stability was shown to be destabilizing for small values of η . As the value of η was increased, however, this effect was shown to be opposed by a stabilizing trend produced by the product-of-inertia parameter K_{XZ} which is a function of K_{Z_0} , K_{X_0} , and η . The stabilizing effect of increasing K_{Z_0} as determined in this investigation is therefore apparently the result of the corresponding increase in K_{XZ} . Additional calculations indicated that, for some smaller values of η (and consequently smaller values of K_{XZ}), increases in K_{Z_0} would have been destabilizing.

The comparison of experimental and theoretical results presented in figure 6 shows that fairly good qualitative agreement was obtained between the theory and experiment. The theoretical results are given in this figure in the form of lines of constant damping which were obtained by cross-plotting and extrapolating the data of figure 5. The flight-test damping ratings indicate the same trends with changes in K_{X_0} and K_{Z_0} as do the calculated lines of constant damping. The theoretical results appear to be somewhat conservative since they indicate instability for two of the flight-test conditions which appeared to be slightly stable. This discrepancy is probably partly the result of using estimated values rather than measured values for some of the stability parameters, in particular, for the vertical-tail contribution to C_{n_p} . A change in the tail contribution to C_{n_p} in the positive direction was found to shift the stability boundary in figure 6 so that stability was indicated for all flight conditions. This change would produce better agreement between the theoretical and experimental results.

Lateral Control

Response to lateral control.- The lateral-control ratings assigned to each of the conditions are listed in table III and are also shown in figure 7. Boundaries have been drawn in figure 7 to enclose the points of equivalent rating. The best response to lateral control was obtained with minimum inertia as shown in this figure and the control characteristics became worse as the moments of inertia were increased. For a given increase in K_{X_0} or K_{Z_0} the reduction in the control rating was about the same.

As K_{X_0} was increased, the rolling acceleration was reduced. This reduction caused a lag in the response of the model to control and

increased the time required for the model to reach a given angle of bank or to return to a wing-level attitude. The model also had a tendency to overshoot after a corrective control was applied so that steady wing-level flight was difficult to attain once the model was disturbed. When K_{Z_0} was increased, the flight behavior appeared to be either better or worse depending upon the magnitude of the disturbance. For small disturbances, the increased yawing inertia tended to delay the building-up of the yawing motion so that the adverse yawing was less than that for the low-inertia condition. For large disturbances, however, there was sufficient time for the yawing motion to build up, and the high inertia tended to keep the model in a yawed attitude and thus made the adverse yawing appear larger. During the flights, even with proper coordination of ailerons and rudder, more difficulty was experienced in controlling the model as the rolling inertia was increased. On the other hand, when the rudder travel was increased along with the yawing inertia, the detrimental effects of increased inertia on the control characteristics could be minimized.

Time histories of the calculated lateral motions of the model produced by a continuously applied rolling moment ($C_l = 0.001$) and by a continuously applied yawing moment ($C_n = 0.001$) are presented in figure 8. The rolling and yawing moments are assumed to be produced by the ailerons and rudder, respectively.

When K_{X_0} is increased by changing from condition I to condition II (fig. 8), the time required to reach a given angle of bank or yaw for a given aileron or rudder deflection is increased. This effect of increasing K_{X_0} is the result of an increase in the time required to reach the final rolling and yawing velocities and is attributed to the reduction of the rolling acceleration as previously mentioned. The magnitude of the final rolling and yawing velocities (as indicated by the slopes of the curves) is apparently not affected by changes in K_{X_0} . The effect of increasing K_{X_0} by changing from condition III to condition IV is not so readily apparent from the curves of figure 8 because of the oscillatory character of the motions.

The effect of increasing K_{Z_0} (changing from condition I to condition III and from condition II to condition IV, fig. 8) is to increase the time required to reach a given angle of bank or yaw as the result of a reduction in the final rolling and yawing velocities. In the initial phase of the motion for the case of the applied rolling moment (fig. 8(a)) this effect is attributed mainly to the product-of-inertia parameter K_{XZ} which increases with increases in K_{Z_0} . (See table III.) With a positive

value of K_{XZ} , a positive rolling acceleration produces a negative yawing moment which increases the adverse sideslip. It is this increased adverse sideslip which (because of the effective dihedral $-C_{l\beta}$ of the model) produces an increased rolling moment opposing the applied rolling moment and therefore causes a reduction in the rolling velocity. Since this incremental adverse rolling moment decreases with time because the difference in sideslip angle between the various conditions does not persist (see fig. 8(a)), this effect does not adequately explain the reduction in the final rolling velocity. This reduction in the final rolling velocity can be attributed, at least partly, to the reduction in yawing velocity with increasing K_{Z_0} . Through the stability derivative C_{lr} (the rolling-moment-due-to-yawing parameter) this reduction in yawing velocity reduces the rolling moment in the direction of rolling and therefore causes a reduction in the rolling velocity. In the case of the applied yawing moment (fig. 8(b)), the motions are somewhat different from those for the case of the applied rolling moment but the effects of K_{Z_0} are similar and can be explained in a similar manner.

The effect of increasing K_{X_0} and K_{Z_0} simultaneously (changing from condition I to condition IV) is to increase the effective time lag in reaching the final rolling and yawing velocities and also to reduce the magnitude of these final velocities. This result is attributed to a combination of the individual effects of K_{X_0} and K_{Z_0} .

Lateral-control coordination.- It was observed during the flight tests that, as the moments of inertia were varied, the coordination between rudder and ailerons had to be changed in order to obtain the most satisfactory control characteristics for each condition. The aileron travel was held constant throughout and control coordination was changed by varying the amount of rudder travel. Optimum combinations of aileron and rudder travel for the flight tests are given in table III. These data reveal that increased rudder travel was required as K_{Z_0} was increased and that for the higher values of K_{Z_0} the ailerons had to be rigged up to reduce the adverse yawing moments of the ailerons. When K_{X_0} was increased, however, the required rudder travel was reduced and at the highest value of K_{X_0} , the rudder was fixed and flights were made with ailerons alone. When the various simultaneous changes in K_{X_0} and K_{Z_0} were made, only very small changes in rudder travel were required.

These trends are apparently related to changes in the nondimensional product-of-inertia parameter K_{XZ} as previously mentioned. For example, the large increase in K_{XZ} caused by increasing K_{Z_0} (changing from condition 1 to condition 3) increased the adverse yawing. On the other hand, the reduction in K_{XZ} caused by increasing the value of K_{X_0} (changing from condition 4 to condition 7) decreased the adverse yawing. In order to illustrate this point the initial portion of some of the yawing motions from figure 8(a) are presented in figure 9 plotted to a larger scale. The data of figure 9 indicate that the rolling acceleration produced by deflected ailerons causes an initial adverse yawing motion for condition I. As K_{Z_0} increases (by changing from condition I to condition III) this adverse yawing motion is increased but as K_{X_0} increases (by changing from condition I to condition II) the motion is reduced. The magnitude of the yawing moment that must be applied simultaneously with the rolling moment to overcome this adverse motion is obviously dependent on the magnitude of the adverse motion. Consequently, the rudder deflections required to produce this yawing moment should increase with K_{Z_0} and decrease with K_{X_0} in the same manner as noted in the flight tests.

General Flight Behavior

The general-flight-behavior ratings assigned to each of the test conditions are listed in table III and are also presented in figure 10. Boundaries enclosing points of equivalent rating are also shown in figure 10. This figure indicates that the best general flight behavior was obtained with minimum K_{X_0} and K_{Z_0} and that the behavior became worse as the moments of inertia were increased. In the case of increasing K_{Z_0} , a comparison of the damping and control ratings with the general-flight-behavior ratings indicates that the deterioration of the lateral control was the predominant factor affecting the pilot's opinion of general flight behavior. In the case of increasing K_{X_0} , the flight behavior became worse as both the damping and the control effectiveness decreased and it was not apparent to the pilot whether one of these factors was more important than the other in producing this trend.

CONCLUDING REMARKS

Results of recent investigations have shown that the effect on dynamic stability of any one particular parameter is usually dependent on other variables entering into the stability equations. The effects of mass distribution on lateral stability and control which were determined in this investigation must therefore be applied only to configurations and conditions generally similar to those used in the flight tests. The effects of mass distribution on the low-speed dynamic lateral stability and control characteristics of the model with a 45° sweptback wing at a lift coefficient of 0.7 as determined in this investigation may be summarized as follows:

1. The damping of the lateral oscillation increased slightly with increasing yawing moment of inertia and decreased with increasing rolling moment of inertia.
2. Increasing the rolling and yawing moments of inertia decreased the response of the model to lateral controls. Increasing the rolling moment of inertia increased the time required to reach final rolling and yawing velocities but did not appreciably affect the magnitude of the final velocities; increasing the yawing moment of inertia, however, decreased the magnitude of these final velocities and increased the time required to reach the final velocities.
3. Increasing the yawing moments of inertia caused an increase in the rudder travel relative to the aileron travel required for smoothly coordinated maneuvers; increasing the rolling moments of inertia, however, caused a decrease in the required rudder travel.
4. The general flight behavior became worse as the rolling and yawing moments of inertia were increased.
5. Fairly good agreement was obtained between the trends predicted by theory and those obtained from the flight tests.

Langley Aeronautical Laboratory
National Advisory Committee for Aeronautics
Langley Field, Va., December 21, 1950

REFERENCES

1. Campbell, John P., and Seacord, Charles L., Jr.: The Effect of Mass Distribution on the Lateral Stability and Control Characteristics of an Airplane as Determined by Tests of a Model in the Free-Flight Tunnel. NACA Rep. 769, 1943.
2. Shortal, Joseph A., and Osterhout, Clayton J.: Preliminary Stability and Control Tests in the NACA Free-Flight Wind Tunnel and Correlation with Full-Scale Flight Tests. NACA TN 810, 1941.
3. Shortal, Joseph A., and Draper, John W.: Free-Flight-Tunnel Investigation of the Effect of the Fuselage Length and the Aspect Ratio and Size of the Vertical Tail on Lateral Stability and Control. NACA ARR 3D17, 1943.
4. Stone, Ralph W., Jr., Burk, Sanger M., Jr., and Bihrlé, William, Jr.: The Aerodynamic Forces and Moments on a $\frac{1}{10}$ -Scale Model of a Fighter Airplane in Spinning Attitudes as Measured on a Rotary Balance in the Langley 20-Foot Free-Spinning Tunnel. NACA TN 2181, 1950.
5. Sternfield, Leonard, and Gates, Ordway B., Jr.: A Simplified Method for the Determination and Analysis of the Neutral-Lateral-Oscillatory-Stability Boundary. NACA Rep. 943, 1949. (Formerly NACA TN 1727.)
6. Toll, Thomas A., and Queijo, M. J.: Approximate Relations and Charts for Low-Speed Stability Derivatives of Swept Wings. NACA TN 1581, 1948.
7. Hassell, James L., and Bennett, Charles V.: The Dynamic Lateral Control Characteristics of Airplane Models Having Unswept Wings with Round- and Sharp-Leading-Edge Sections. NACA TN 2219, 1950.
8. Jones, Robert T.: A Simplified Application of the Method of Operators to the Calculation of Disturbed Motions of an Airplane. NACA Rep. 560, 1936.
9. Jones, Robert T.: The Influence of Lateral Stability on Disturbed Motions of an Airplane with Special Reference to the Motion Produced by Gusts. NACA Rep. 638, 1938.
10. Zimmerman, Charles H.: An Analysis of Lateral Stability in Power-Off Flight with Charts for Use in Design. NACA Rep. 589, 1937.
11. Sternfield, Leonard: Some Considerations of the Lateral Stability of High-Speed Aircraft. NACA TN 1282, 1947.

TABLE I
PHYSICAL CHARACTERISTICS OF MODEL

Weight, lb	8.64
Wing loading, W/S, lb/sq ft	4.32
Relative-density factor, μ_b	20
Center-of-gravity location, percent \bar{c}	22
Inclination of principal axes of inertia to body axes, ϵ , deg	0
Wing:	
Airfoil section, perpendicular to 0.25-chord line	Rhode St. Genese 35 (12 percent thick)
Area, sq ft	2.01
Span, ft	2.83
Aspect ratio	4
Sweepback, leading edge, deg	45
Dihedral, deg	0
Taper ratio	0.6
Mean aerodynamic chord, \bar{c} , ft	0.72
Location of leading-edge mean aerodynamic chord behind leading-edge root chord, ft	0.65
Root chord, ft	0.89
Tip chord, ft	0.53
Aileron:	
Span	Semispan
Chord	0.20 chord perpendicular to 0.25-chord line
Horizontal tail:	
Area, sq ft	0.38
Span, ft	1.17
Taper ratio	0.50
Vertical tail:	
Area, sq ft	0.10
Span, ft	0.45
Taper ratio	0.50
Aspect ratio	2.0

TABLE II
 MASS AND AERODYNAMIC PARAMETERS USED TO CALCULATE
 CHARACTERISTICS OF THE LATERAL MOTION

μ_b	20
K_{X_0}	0.107 to 0.225
K_{Z_0}	0.216 to 0.600
ϵ , deg	0
C_L	0.7
α , deg	16
η , deg	16
γ , deg	-17
$m/\rho SV$, sec	0.859
l/b	0.55
z/b	0.077

Parameter	Wing + fuselage	Tail	Total
C_{l_β}	-0.223	0	-0.223
C_{n_β}	0.028	0.114	0.142
C_{y_β}	-0.052	-0.212	-0.264
C_{l_p}	-0.290	0	-0.290
C_{n_p}	-0.040	-0.036	^a -0.076
C_{y_p}	0.300	0	0.300
C_{l_r}	0.175	^b 0.018	0.193
C_{n_r}	-0.037	^b -0.124	-0.161
C_{y_r}	0	0	0

^aValue of -0.044 used in calculations for the lateral motions presented in figure 8.

^bTail contributions were determined from the following equations:

$$C_{l_{r\text{tail}}} = -2 \frac{l}{b} \frac{z}{b} C_{y_\beta \text{tail}}$$

$$C_{n_{r\text{tail}}} = 2 \left(\frac{l}{b} \right)^2 C_{y_\beta \text{tail}}$$



TABLE III
RESULTS OF FLIGHT TESTS

Condition	Type of change	K_{X_0}	K_{Z_0}	K_{XZ}	Oscillatory-damping rating (a)	Lateral-control rating (a)	General-flight-behavior rating (a)	Optimum combinations of -	
								δ_a (deg)	δ_r (deg)
1		0.122	0.327	0.0244	A-	B	A-	± 20	± 22
2	K_{Z_0} increased	.122	.446	.0487	A	C	B	15 -25	± 44
3		.122	.579	.0849	A+	D	D	12 -28	± 44
4		.142	.219	.0074	B	A	A	± 20	± 22
5	K_{X_0} increased	.156	.219	.0063	B	A	B	± 20	± 10
6		.197	.219	.0024	C	B	C	± 20	± 10
7		.224	.219	-.0006	C-	B	C	± 20	0
4		.142	.219	.0074	B	A	A	± 20	± 22
8	Both K_{X_0} and K_{Z_0} increased	.155	.322	.0211	B	B	B	± 20	± 15
9		.203	.322	.0166	C	B	C	± 20	± 15
10		.197	.420	.0365	C	C	C	± 20	± 15

^sRatings defined on page 7.



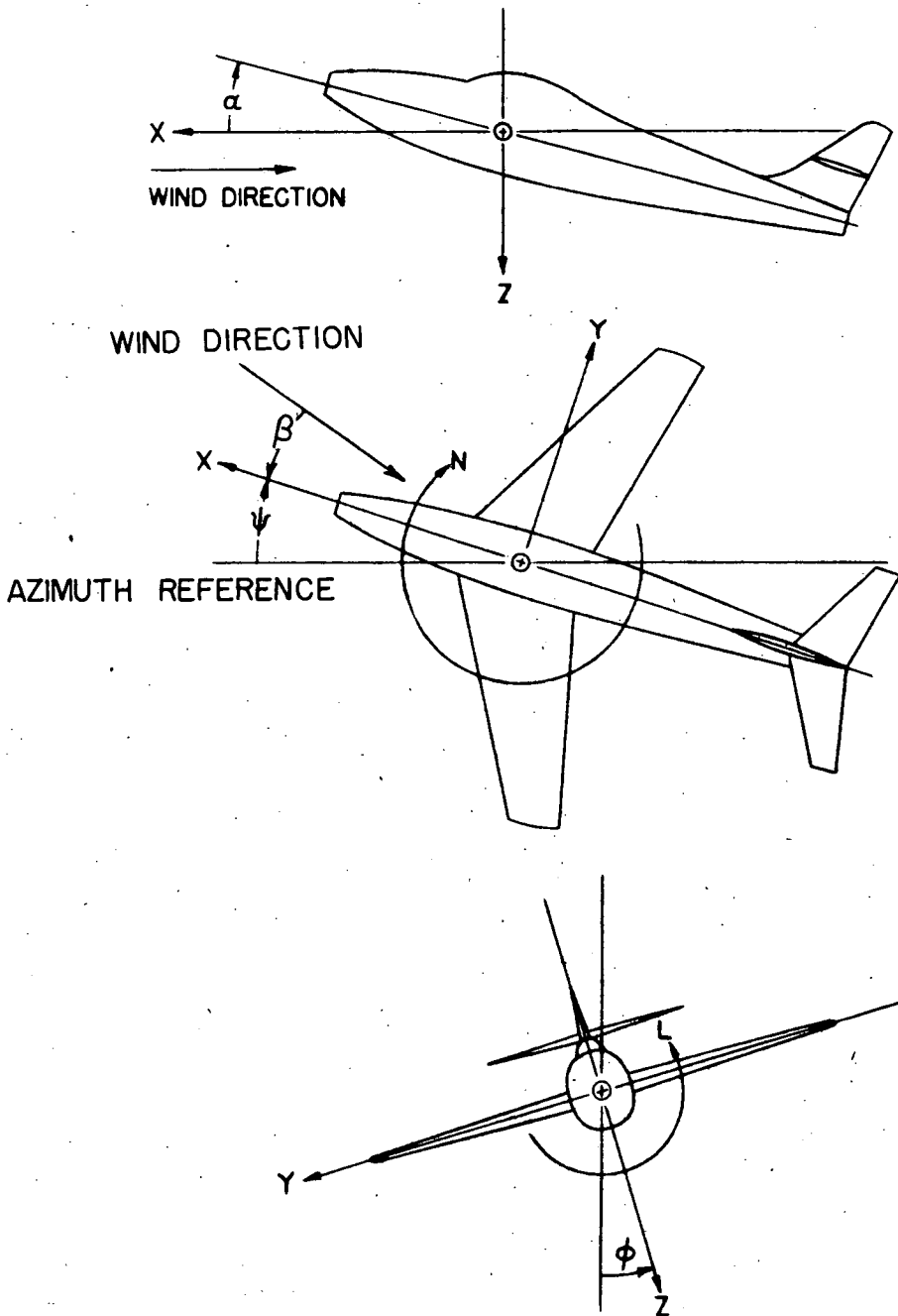


Figure 1.- Stability system of axes. Arrows indicate positive directions of moments, forces, and angles. This system of axes is defined as an orthogonal system having the origin at center of gravity and in which Z-axis is in plane of symmetry and perpendicular to relative wind, X-axis is in plane of symmetry and perpendicular to Z-axis, and Y-axis is perpendicular to plane of symmetry.

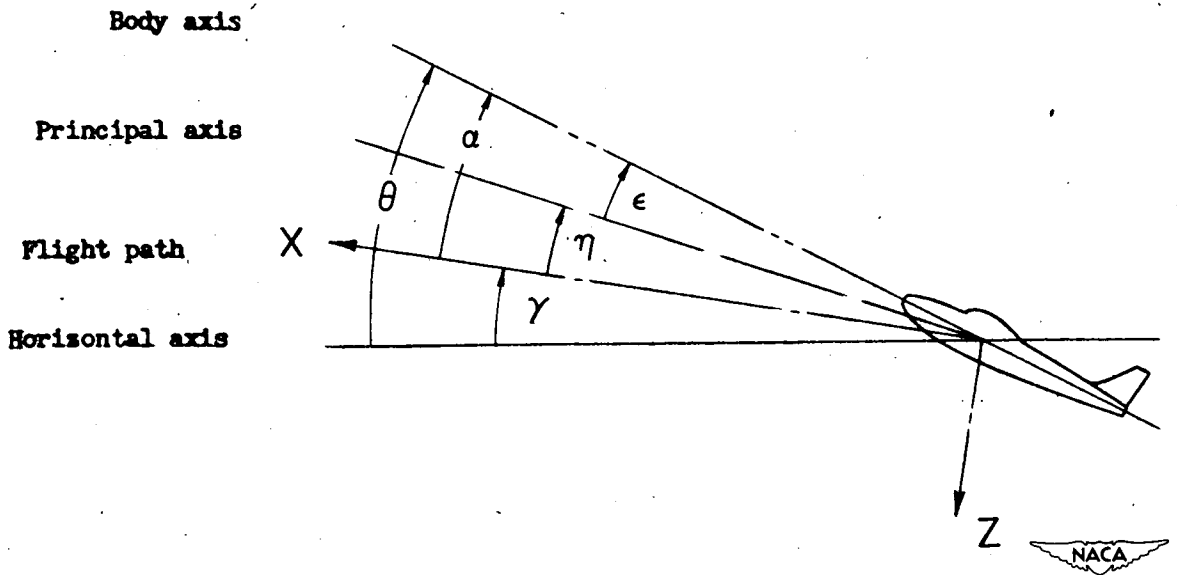


Figure 2.- System of axes and angular relationship in flight. Arrows indicate positive direction of angles. $\eta = \theta - \gamma - \epsilon$.

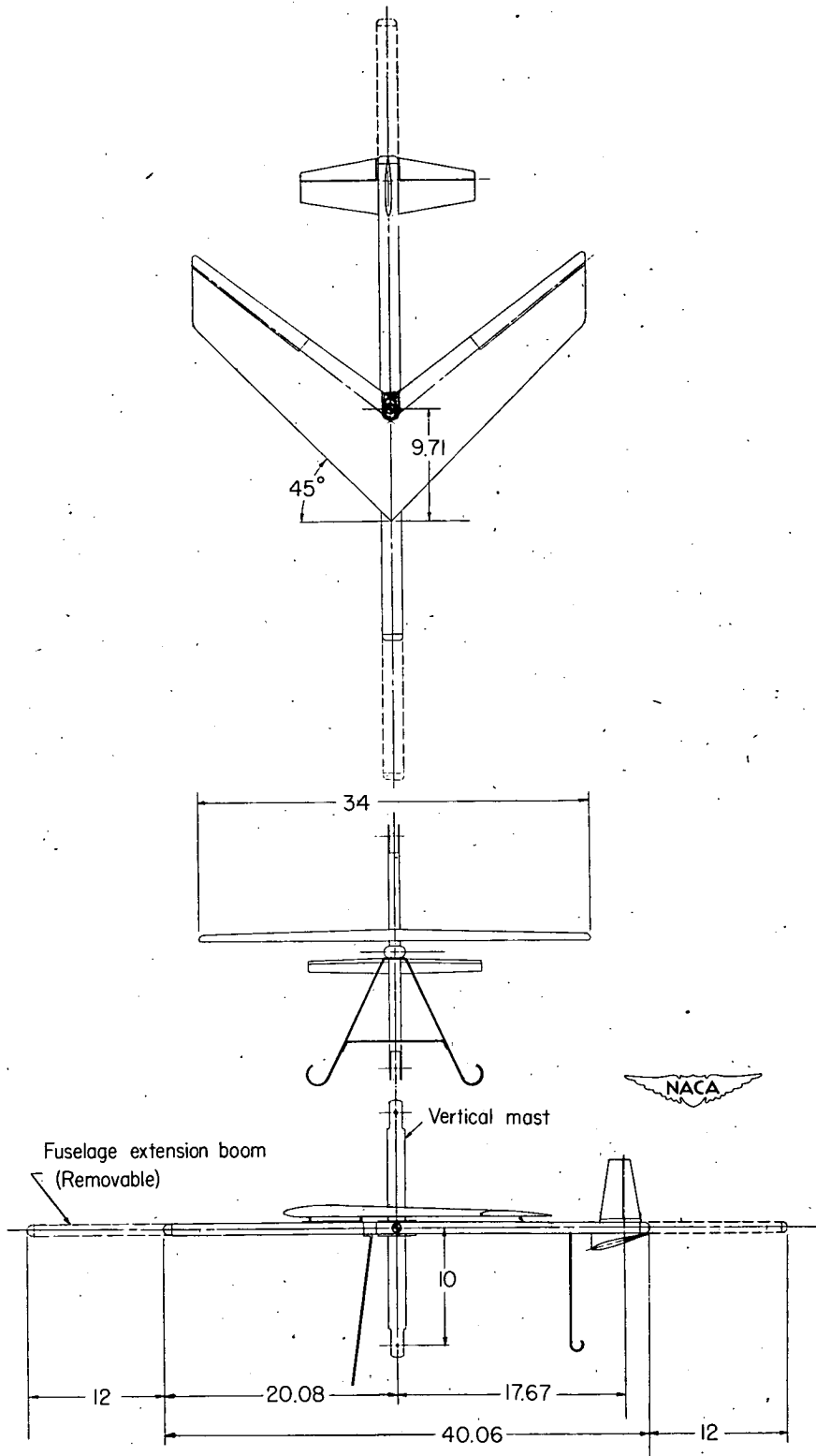


Figure 3.- Three-view drawing of model tested in Langley free-flight tunnel. (All dimensions are in inches.)

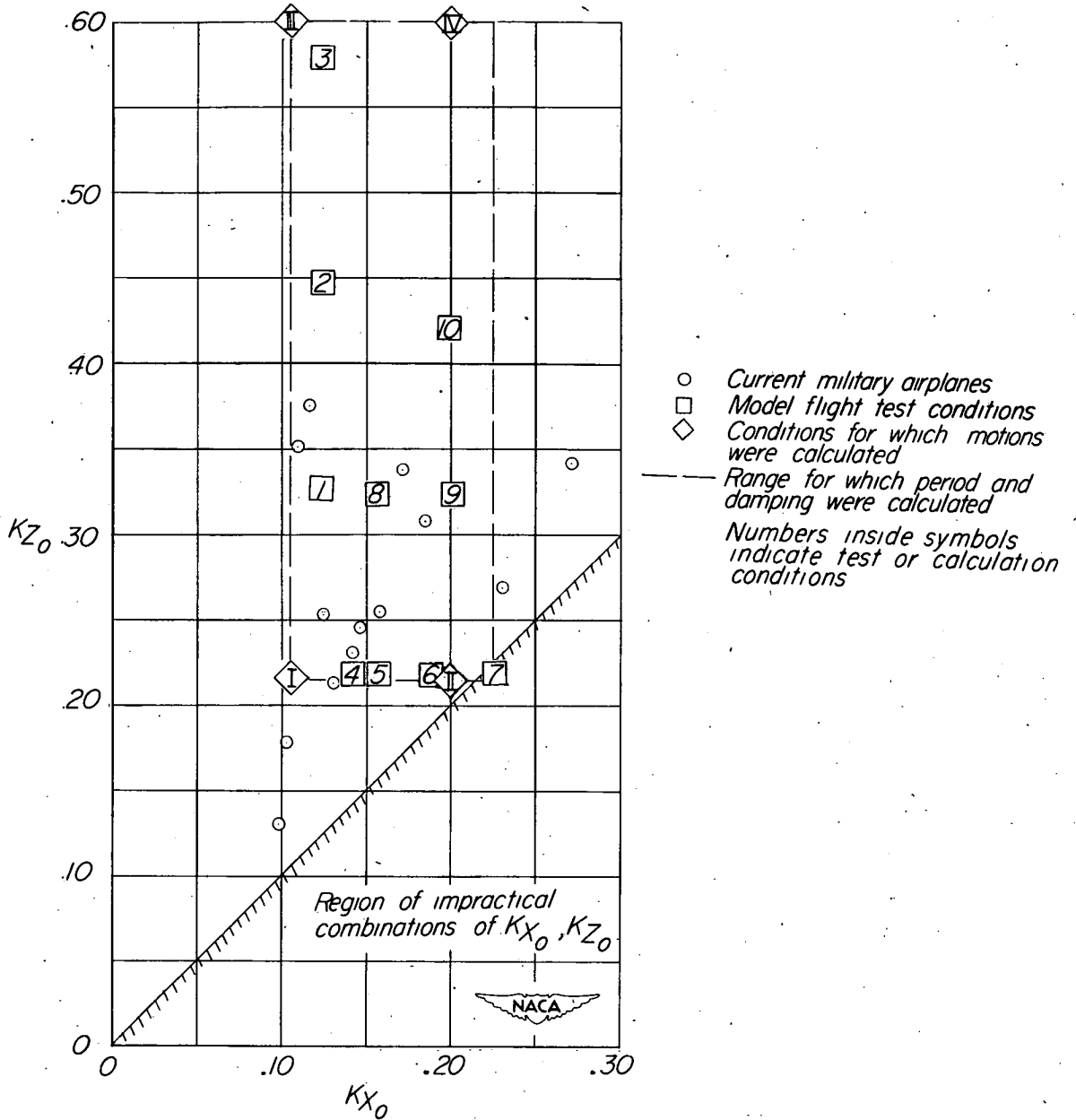


Figure 4.- Range of values for mass-distribution parameters, K_{X_0} and K_{Z_0} , covered in investigation compared with values for several current military airplanes.

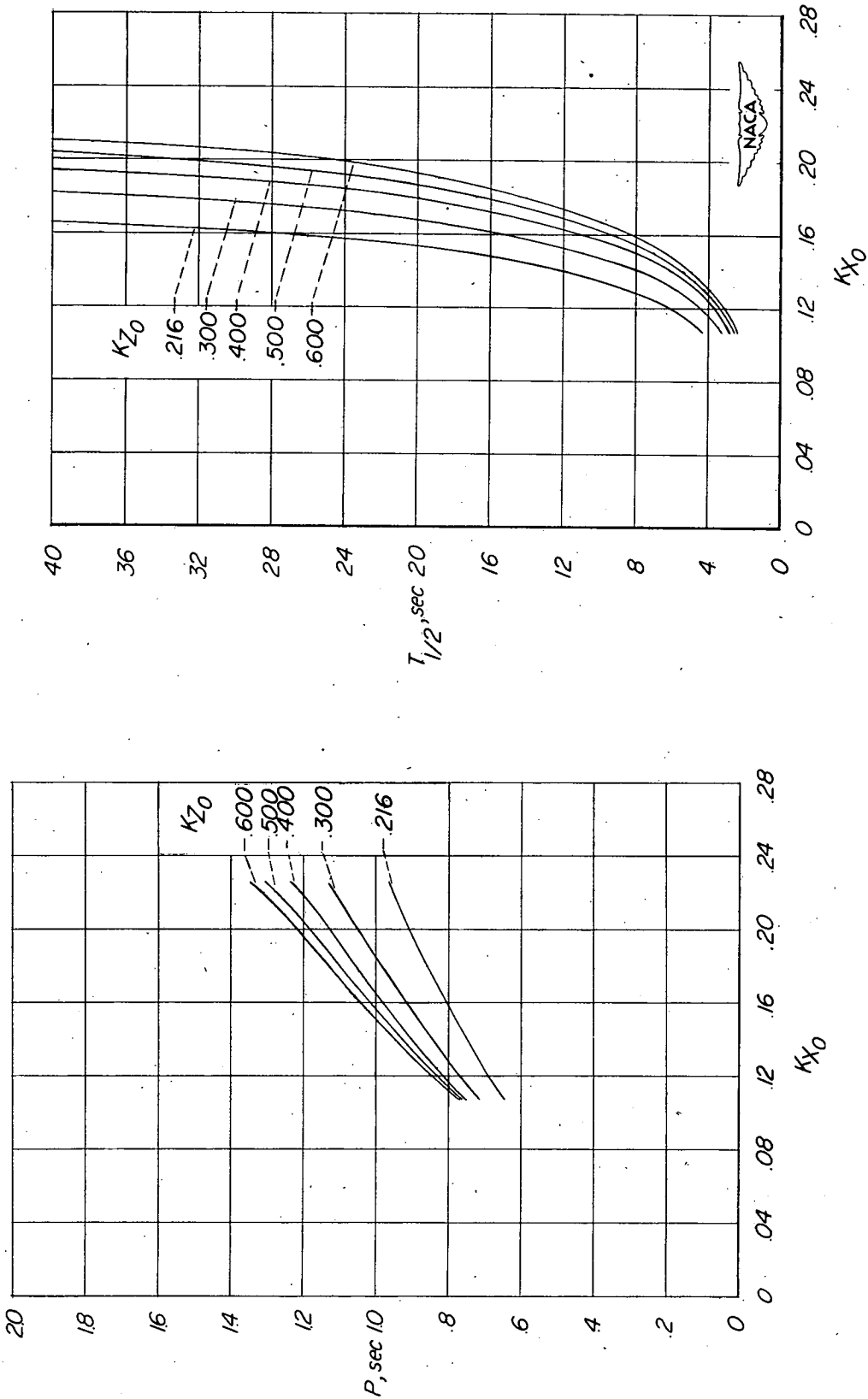


Figure 5.-- Calculated period and time to damp to one-half amplitude of lateral oscillatory mode of model motions.

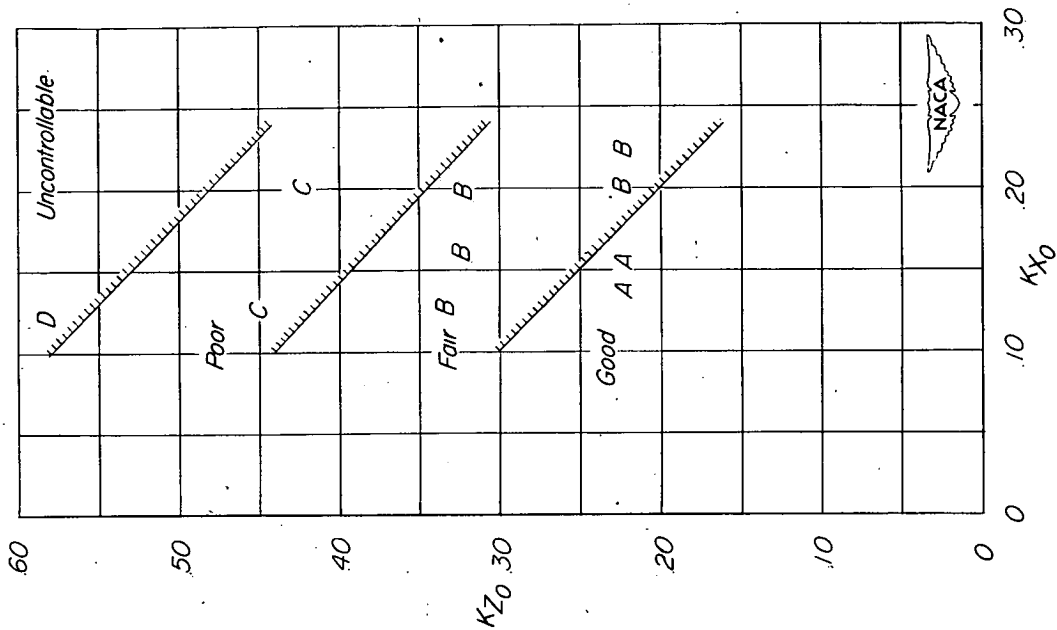


Figure 7.- Flight-test ratings for lateral control effectiveness.

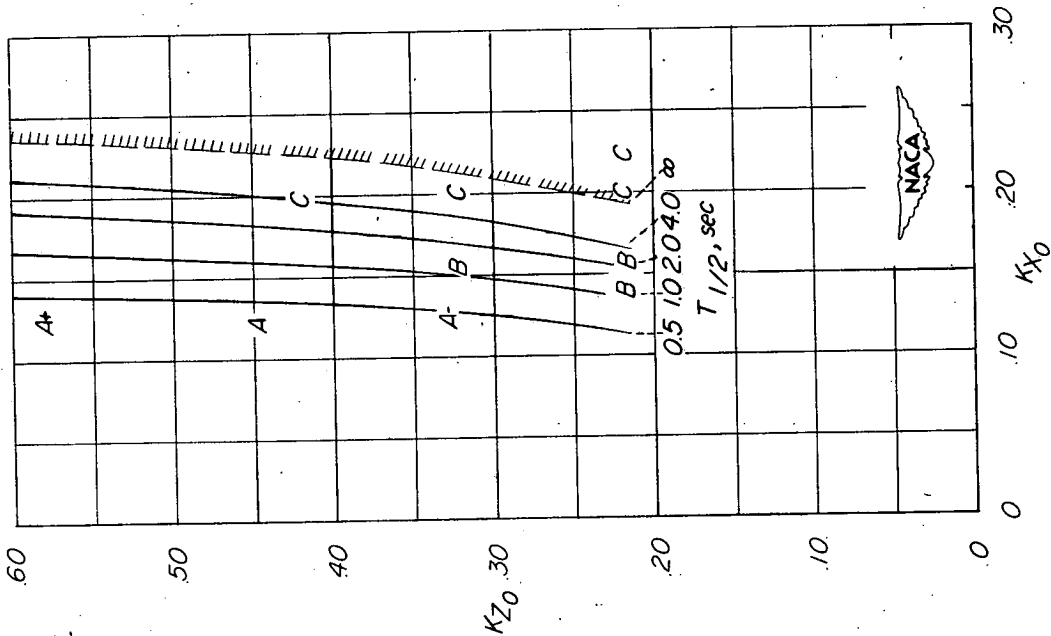
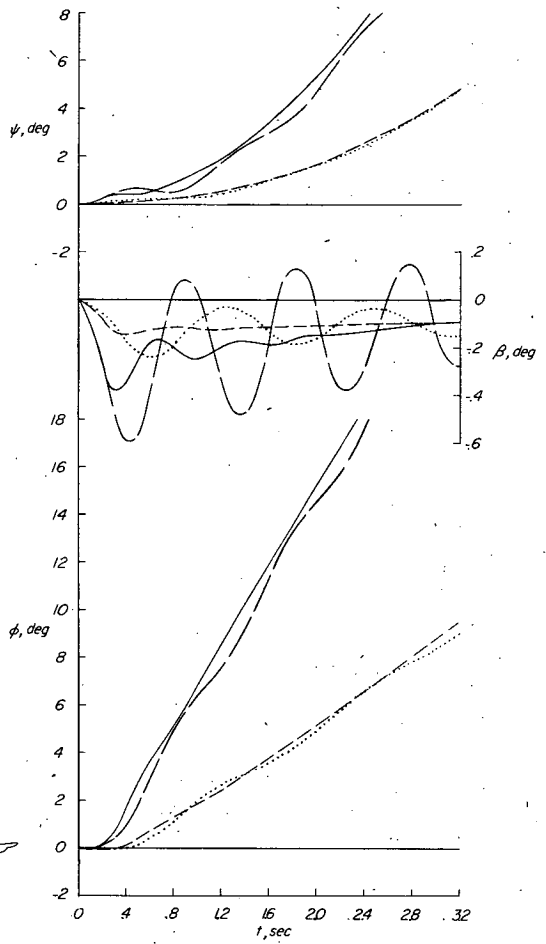
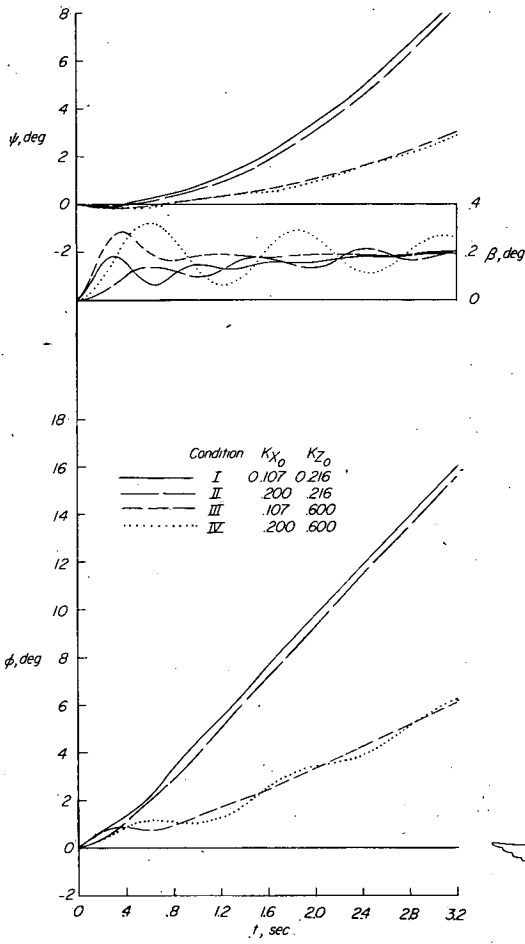


Figure 6.- Lines of constant damping (calculated $T_{1/2}$) compared with flight-test damping ratings.



(a) Continuously applied rolling moment ($C_l = 0.001$) produced by deflected ailerons.

(b) Continuously applied yawing moment ($C_n = 0.001$) produced by deflected rudder.

Figure 8.- Time histories of calculated rolling and yawing motions of model showing effects of moments of inertia on effectiveness of lateral controls.

Condition	K_{X_0}	K_{Z_0}	K_{XZ}
————— I	0.107	0.216	0.0094
————— II	.200	.216	.0018
- - - - - III	.107	.600	.0924

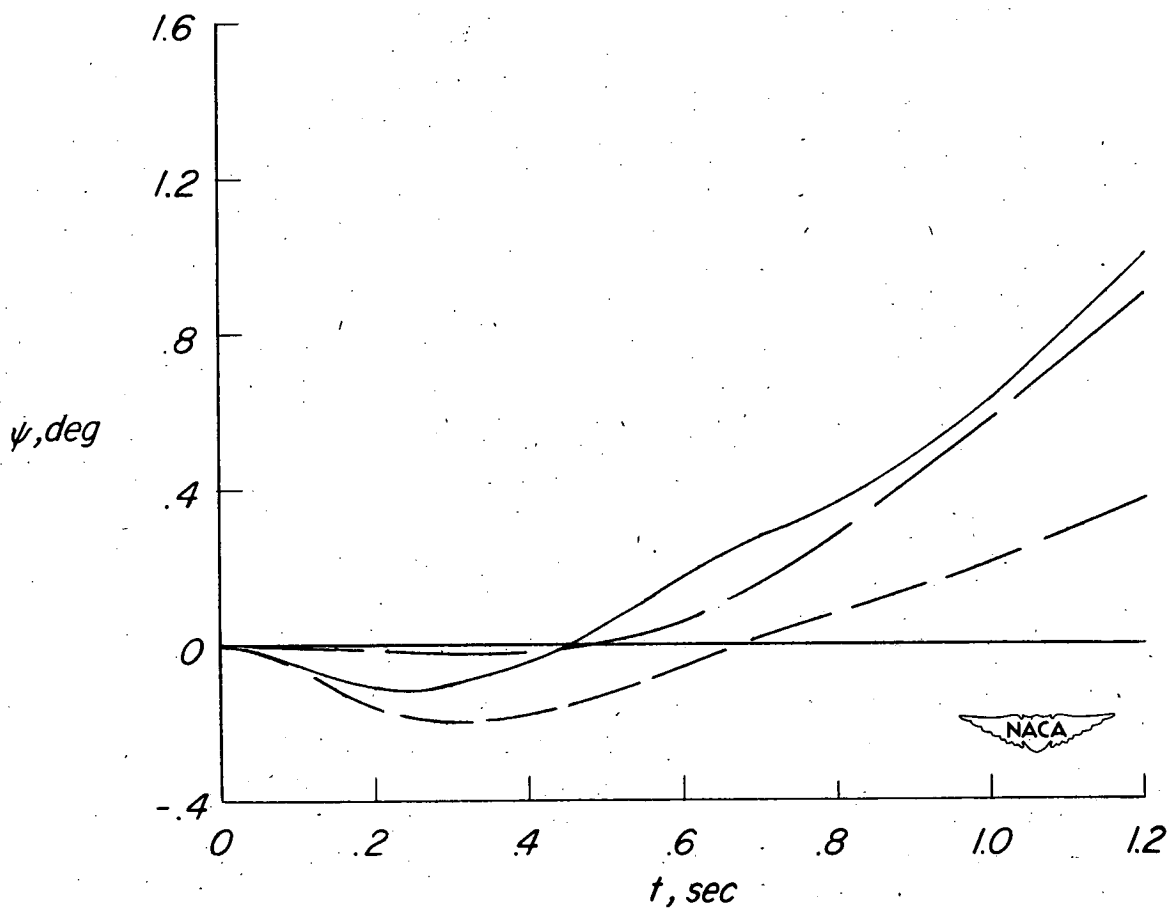


Figure 9.- Time histories of calculated yawing motions of model produced by a continuously applied rolling moment ($C_l = 0.001$) showing effects of moment of inertia on initial adverse yawing motion. (Initial portion of curves of fig. 8(a).)

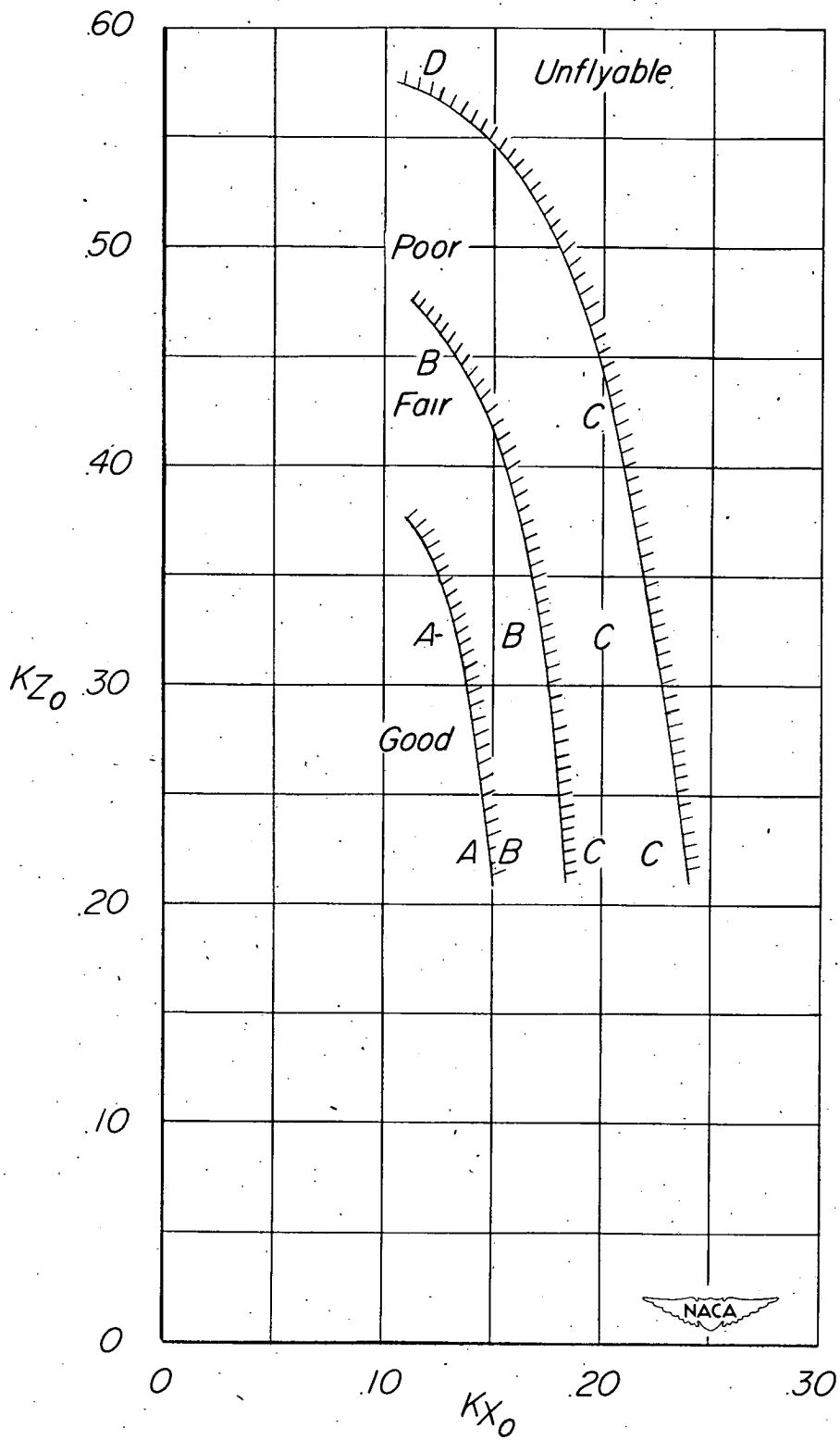


Figure 10.- Flight-test ratings for general flight behavior.